Biosensors and Bioelectronics 133 (2019) 86–93

Contents lists available at ScienceDirect

Biosensors and Bioelectronics

journal homepage: www.elsevier.com/locate/bios

Label-free impedimetric immunosensor based on arginine-functionalized gold nanoparticles for detection of DHEAS, a biomarker of pediatric adrenocortical carcinoma

Dhésmon Lima[a], Juliana Inaba[a], Luma Clarindo Lopes[a], Giselle Nathaly Calaça[b], Patrícia Los Weinert[a], Rafaela Lenzi Fogaça[c], Juliana Ferreira de Moura[c], Larissa Magalhães Alvarenga[c], Bonald Cavalcante de Figueiredo[d,e], Karen Wohnrath[a], Christiana Andrade Pessôa[a,*]

[a] Department of Chemistry, Universidade Estadual de Ponta Grossa, Av. General Carlos Cavalcanti, 4748, 84030-900 Ponta Grossa, Paraná, Brazil
[b] Department of Chemistry, Instituto Federal do Paraná, Rodovia PR 323, KM 310, 87507-014 Umuarama, Paraná, Brazil
[c] Department of Basic Pathology, Universidade Federal do Paraná, Av. Coronel Francisco H. dos Santos, 100, 81530-000 Curitiba, Paraná, Brazil
[d] Department of Community Health, Universidade Federal do Paraná, Rua Padre Camargo, 261, 80069-240 Curitiba, Paraná, Brazil
[e] Instituto de Pesquisa Pelé Pequeno Príncipe, Av. Silva Jardim, 1632, 80250-060 Curitiba, Paraná, Brazil

ARTICLE INFO

Keywords:
Impedimetric immunosensor
Dehydroepiandrosterone sulfate
Pediatric adrenocortical carcinoma
Gold nanoparticles
Factorial design
Response surface methodology

ABSTRACT

Pediatric adrenocortical carcinoma (pACC) is a rare and aggressive malignancy of high occurrence in Southern Brazil. pACC is characterized by the usual overproduction of dehydroepiandrosterone sulfate (DHEAS), whose detection in serum or plasma can be effective to the early diagnosis of the disease. Therefore, the present paper reports, for the first time, the construction and application of a label-free impedimetric immunosensor to detect DHEAS, which was based on the modification of an oxidized glassy carbon electrode with arginine-functionalized gold nanoparticles (AuNPs-ARG) and anti-DHEA IgM antibodies (*ox*-GCE/AuNPs-ARG/IgM). AuNPs-ARG was synthesized by a green route, and characterized by UV–VIS spectroscopy, FTIR, TEM, DLS, and XRD. The construction of *ox*-GCE/AuNPs-ARG/IgM was optimized through factorial design and response surface methodology. Cyclic voltammetry and electrochemical impedance spectroscopy measurements were employed to characterize the optimized immunosensor. The DHEAS detection principle was based on the variation of charge transfer resistance (ΔR_{ct}) relative to the $Fe(CN)_6^{4-/3-}$ electrochemical probe after immunoassays in the presence of the biomarker. A linear relationship between ΔR_{ct} and DHEAS concentration was verified in the range from 10.0 to 110.0 μg dL^{-1}, with a LOD of 7.4 μg dL^{-1}. Besides the good sensitivity, the immunosensor displayed accuracy, stability, and specificity to detect DHEAS. The promising analytical performance of *ox*-GCE/AuNPs-ARG/IgM was confirmed by quantifying DHEAS in real patient plasma samples, with results that were comparable to the reference chemiluminescence assay. Our results suggest that the presented immunosensor can find clinical applications in the early diagnosis of pACC and to monitor DHEAS levels in other adrenal pathologies.

1. Introduction

The development of new systems for the detection of clinically relevant analytes has attracted the attention of researchers from several fields, who continually strive for the construction of sensitive, selective, and low-cost devices that can detect such compounds in biological samples with good accuracy and precision (Pires et al., 2014). Particularly, electrochemical immunosensors are among the most studied ones, since such devices combine the high specificity of antibodies with advantages such as sensitivity and fast response. Moreover, the possibility of miniaturization and in situ detection make these biosensors promising for applications in point-of-care diagnostics (Rama and Costa-García, 2016; Wan et al., 2013).

In most cases, the electrical signal generated by the transduction process after the interaction between immunoglobulins and antigens can be amplified by co-immobilizing nanostructured materials on the

* Corresponding author.
E-mail address: christiana.pessoa@pq.cnpq.br (C. Andrade Pessôa).

https://doi.org/10.1016/j.bios.2019.02.063
Received 10 February 2019; Accepted 23 February 2019
Available online 06 March 2019
0956-5663/

immunosensor surface. Besides this, the use of nanomaterials such as graphene, carbon nanotubes, quantum dots, and noble metal nanoparticles in immunosensor construction usually provides a better attachment of antibodies to the electrode due to their high surface area. This can facilitate the access of antigens to the active sites of the immobilized antibodies, increasing the efficiency of the transduction process and improving the device sensitivity. (Devi et al., 2015).

The properties displayed by gold nanoparticles (AuNPs) make them one of the most suitable nanomaterials for the construction of electrochemical immunosensors. These features include easy preparation, possibility of functionalization, high electrical conductivity, high surface area, and biocompatibility (Saha et al., 2012). The interaction between AuNPs and biomolecules occur through electrostatic interactions, van der Waals forces, and covalent binding to specific groups, which allow this nanomaterial to be exploited as an efficient platform for immobilizing antibodies, antigens and other proteins without losing their bioactivity (Austin et al., 2014). Therefore, the usage of AuNPs in the construction of immunosensors can provide ultrasensitive devices with good analytical performances at detecting disease-related analytes, such as biomarkers (Carneiro et al., 2017; Chen et al., 2018; Karaboğa et al., 2016; Kumar et al., 2016; Luna et al., 2015; Sun et al., 2017).

Adrenocortical carcinoma (ACC) is an aggressive neoplastic disease of high malignant potential, which is derived from cells of the adrenal cortex. This disease usually presents a poor prognosis, with an average 5-year survival rate around 20–40% in stages III and IV (Doghman et al., 2010; Ronchi et al., 2014; Lalli and Figueiredo, 2015). Among adults, ACC has a general worldwide incidence of 0.7–2.0 cases per million population per year, but it is rarer in children younger than 15 years of age, in which an incidence of only 0.2–0.3 per million per year is observed (Fassnacht et al., 2011; Lalli and Figueiredo, 2015). However, an unusually high annual incidence of pediatric ACC (pACC) has been found in southern Brazil (2.9–4.2 cases per million per year, around 15-fold higher than the global average), due to the endemic germline *TP53* R337H mutation that is quite frequent in that population (Ribeiro et al., 2001). For example, the *TP53* R337H prevalence is 0.27% in the population of Paraná state, and it was estimated that approximately 200,000 carriers live in southern and southeastern Brazilian states (Custódio et al., 2013). This mutation is directly associated to a specific dysfunction of p53 protein (DiGiammarino et al., 2002), which is involved in DNA repair mechanisms (Fett-Conte and Salles, 2002).

Considering the absence of specific cancer-related early symptoms, approximately 70% of patients are diagnosed with pACC at advanced stages, in which the chances of cure are really small (Fay et al., 2014). For instance, the average survival rate for a metastatic disease at the time of diagnosis is less than a year (Ayala-Ramirez et al., 2013). Consequently, due to its malignant and metastatic potential, the early diagnosis of pACC is extremely important.

One of the most prominent characteristics of pACC is the overproduction of adrenal hormones, mainly dehydroepiandrosterone (DHEA) and its sulfate derivative, dehydroepiandrosterone sulfate (DHEAS), which are considered as genuine pACC biomarkers (Fig. S1). This overproduction occurs due to the inefficient steroidogenesis that takes place in malignant neoplasms, leading to the release of steroids precursors such as DHEA and DHEAS (Cavagnini et al., 2016). Therefore, the determination of plasma levels of such steroids can be an effective tool to help in the early diagnosis of pACC.

Some analytical methods have been employed to monitor the concentration of DHEA and DHEAS mainly in blood serum samples, such as HPLC and GC-MS (Abdel-Khalik et al., 2013), LC-MS/MS (Büttler et al., 2015; Chadwick et al., 2005; Damgaard-Olesen et al., 2016; Sánchez-Guijo et al., 2015; Shibata et al., 2015), chemiluminescence (Arakawa et al., 1981; Dennedy et al., 2017; Guran et al., 2015), and ELISA (Lewis et al., 1996; Shrivastav et al., 2011a, 2011b). In spite of their good performance, such techniques are often time consuming and also require expensive instrumentation and labor-intensive sample preparation procedures (Pires et al., 2014; Monerris et al., 2016). Hence, due to the advantages previously mentioned, electrochemical immunosensors may lead to more simple and cheaper methodologies to detect DHEA and DHEAS. For that reason, the present study aimed to construct a sensitive, selective and feasible AuNPs-based immunosensor to detect DHEAS in blood plasma samples, in order to provide an alternative method to the early diagnosis of pACC. To the best of our knowledge, this is the first work that report the application of an electrochemical immunosensor to DHEAS determination. A regular determination pACC-related hormones may also be useful as a strategy of postoperative follow-up of patients, as it may provide consistent evidences of a possible recurrence of the disease (Else et al., 2014; Fassnacht et al., 2011; Przytulska et al., 2015).

2. Material and methods

2.1. Chemicals and solutions

All reagents were of analytical grade and used as received. L-arginine (ARG), $HAuCl_4{\cdot}3H_2O$, D-glucose, $K_4[Fe(CN)_6]{\cdot}3H_2O$, $K_3[Fe(CN)_6]$, bovine serum albumin (BSA), cholesterol, testosterone, progesterone, 1-ethyl-3-(3-dimethylaminopropyl)carbodiimide hydrochloride (EDC), and *N*-hydroxysuccinimide (NHS) were purchased from Sigma-Aldrich (USA). DHEAS was purchased from Steraloids (USA). Fetal bovine serum (FBS; Gibco) was acquired from Thermo Fisher Scientific (USA). Anti-DHEA IgM monoclonal antibodies were obtained and provided by Fogaça et al. (2019).

Sterile 0.15 mol L^{-1}phosphate-buffered saline solution (PBS) at pH 7.4 was used to prepare protein (IgM and BSA) and hormone solutions. Previously to the construction of the immunosensor, the carboxylate moieties of the IgM molecules were chemically activated by using EDC and NHS (50 and 25 mmol L^{-1}, respectively) (Silva et al., 2013; Wang et al., 2011).

2.2. Synthesis and characterization of L-arginine-functionalized gold nanoparticles (AuNPs-ARG)

L-arginine-functionalized gold nanoparticles (AuNPs-ARG) were employed as the electrode modifier to prepare DHEAS immunosensors. Colloidal AuNPs-ARG were synthesized through a green procedure, by the reduction of tetrachloroaurate (III) complex ($[AuCl_4]^-$) with D-glucose, in the presence of ARG. The synthesis protocol (adapted from the work reported by Kumar and Upadhyay, 2016) and the AuNPs-ARG characterization procedures are described in Supplementary Material.

2.3. Immunosensor preparation

Initially, glassy carbon electrodes (geometric area = 3,1 mm^2) were polished with alumina slurry (0.3 μm) on pads moistened with distilled water. After this step, the electrodes were washed with distilled water and sonicated in absolute ethanol for 5 min.

The fabrication process of the immunosensors consisted in the five steps showed in Scheme 1 (see Supplementary Material for a detailed description). The immunosensor was designated as *ox*-GCE/AuNPs-ARG/IgM.

2.4. Immunosensor and immunoassay optimization

The experimental variables, IgM solution concentration ([IgM]), incubation time of the electrodes in IgM solution ($time_{inc}$) and immunoassay temperature (T) were optimized through multivariate techniques, by using factorial designs and response surface methodology (RSM). The evaluated response was the percentage variation of the charge transfer resistance (ΔR_{ct}), which was obtained by electrochemical impedance spectroscopy (EIS) (Section 2.5) after performing

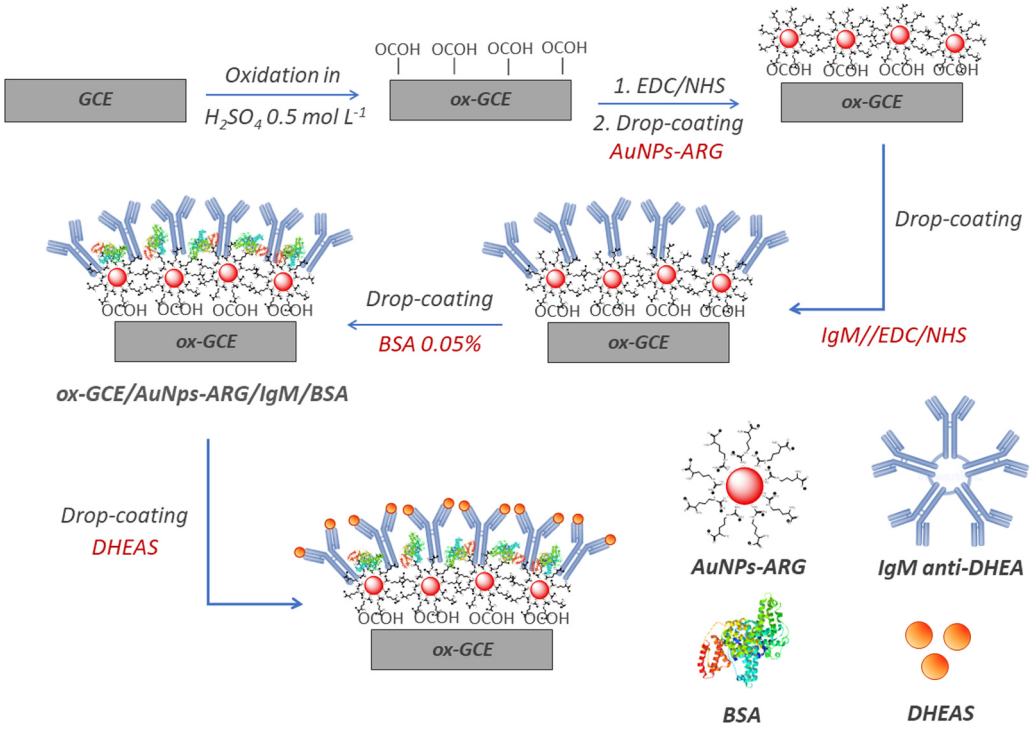

Scheme 1. Schematic representation of the stepwise fabrication procedure of DHEAS immunosensor (in order to make the Scheme clearer, IgM molecules were represented as monomers).

immunoassays with 150 μg dL^{-1} DHEAS. To calculate ΔR_{ct} values, the following equation was employed:

$$\Delta R_{ct} = \left(\frac{R_{ct(imr)} - R_{ct(ims)}}{R_{ct(ims)}} \right).100\%$$

where $R_{ct\ (imr)}$ is the R_{ct} value obtained after the immunoassay and $R_{ct\ (ims)}$ refers to the R_{ct} value presented by the immunosensor before the immunoreaction. The data processing was carried out by using *Statistica*® 13.0 software.

A 2^3 full factorial design (central point assayed in triplicate) was carried out to perform a variable screening and check the influence of each one on the evaluated response. The studied levels of the variables, based on preliminary tests, were: [IgM] = 1.0 (−1), 5.0 (0), and 10.0 μg mL^{-1} (+1); $time_{inc}$ = 30 (−1), 60 (0), and 90 min (+1); and T = 27.0 (−1), 32 (0), and 37 °C (+1). The optimization was continued by performing a 2^2 central composite design (CCD) and RSM. In this step, the variables [IgM] and incubation time were studied in the following levels: [IgM] = 0.15 (−1.41), 0.4 (−1), 1.0 (0), 1.6 (+1), and 1.85 μg mL^{-1} (+1.41); $time_{inc}$ = 48 (−1.41), 60 (−1), 90 (0), 120 (+1), and 132 min (+1.41). In these immunoassays, T was maintained constant at 37 °C. The optimized experimental conditions were then employed to obtain analytical curves for DHEAS determination, in the range from 10.0 to 110.0 μg dL^{-1}.

2.5. Electrochemical measurements

All electrochemical experiments were performed at room temperature, by using a conventional three-electrode cell system. A saturated Ag/AgCl electrode, a platinum spiral wire and the *ox*-GCE/AuNPs-ARG/IgM were employed as reference, auxiliary and working electrodes, respectively. Cyclic voltammetry (CV) and EIS experiments were carried out in an Autolab PGSTAT 100 potentiostat/galvanostat, using 0.15 mol L^{-1} PBS solution containing 10.0 mmol L^{-1} $Fe(CN)_6^{3-}$/$Fe(CN)_6^{4-}$ as supporting electrolyte. A potential window of − 0.3 to + 0.8 V and a scan rate of 50 mV s^{-1} were employed in the CV measurements. For EIS analysis, a 10 mV amplitude sine wave was applied to the electrodes at open circuit potential in the frequency range of 10 kHz to 100 mHz. Nyquist diagrams were fitted by using the equivalent circuit methodology with *Nova*® 2.0 software.

Limit of detection (LOD), sensitivity, reproducibility, and accuracy parameters for DHEAS determination by EIS were determined for the developed immunosensor following the Brazilian Health Surveillance Agency (ANVISA) and International Conference on Harmonization (ICH) guidelines (ANVISA, 2003; ICH, 2005).

2.6. Clinical samples

The plasma samples used in this work were collected from patients of Pequeno Príncipe Hospital (Curitiba, Paraná state, Brazil), and the corresponding DHEAS levels were first determined by chemiluminescence (Pelé Pequeno Príncipe Research Institute, unpublished data). Details regarding to sample preparation and the corresponding immunoassays with the *ox*-GCE/AuNPs-ARG/IgM for DHEAS detection are given in Supplementary Material.

3. Results and discussion

3.1. AuNPs-ARG characterization

L-arginine amino acid has been used both as a capping and functionalizing agent for AuNPs synthesis due to its biocompatible nature and presence of carboxyl, amino, and guanidine moieties in its chemical structure (Fig. S2), which allow the establishment of interactions with biomolecules and functionalized surfaces (Guan et al., 2015; Yang et al., 2011; Zare et al., 2012; Zhang et al., 2018). Herein, ARG was selected to functionalize AuNPs mainly due to the fact that the NH_2 groups can covalently bind (via amide bond) to COO^- groups (Wang et al., 2011). This enabled the AuNPs-ARG to interact with the *ox*-GCE surface and with the Fc fragments of IgM antibodies.

The formation of AuNPs-ARG was evidenced by a solution color change, from yellow ($AuCl_4^-$) to ruby red (AuNPs). D-glucose have been applied as a reducing agent in AuNPs synthesis (Engelbrekt et al.,

2009; Pacławski et al., 2012; Suvarna et al., 2017; Mayya et al., 2004) due to the presence of an aldehyde group in its structure, which is exposed when the molecule is in the linear (open-chain) form. This group is readily oxidized to a carboxylate group in alkaline medium (Nelson and Cox, 2005), with the consequent reduction of $AuCl_4^-$ ion to yield AuNPs. Besides the basic conditions, the heating process can have favored the reduction reaction, probably by shifting the linear ⇌ ring equilibrium in direction to the open-chain form.

The UV–VIS spectrum of the AuNPs-ARG suspension and 100.0 mmol L^{-1} ARG and 0.50 mmol L^{-1} $AuCl_4^-$ solutions are presented in Fig. S3A. ARG spectrum did not present any absorption in 350–400 nm range, whereas a strong absorption band at 301 nm was observed for $AuCl_4^-$, which corresponds to the ligand-to-metal charge transfer transition (LMCT) between gold atom and chloride ligands (Liang et al., 2010). The AuNPs-ARG suspension spectrum displayed a band at 526 nm, which is due to their typical surface plasmon resonance phenomena. The absence of the LMCT band related to the precursor complex in the AuNPs-ARG spectrum suggests that all $AuCl_4^-$ ions initially present were reduced to Au°.

The FTIR spectrum of ARG showed absorption bands at 3367 (νNH_2), 1695 ($\nu C{=}O$), 1581 (νCOO^-), and 1190 (νC-N) (Pretsch et al., 2009). These absorptions shift in AuNPs-ARG spectrum (3516, 1681, 1587, and 1114 cm^{-1} for νNH_2, $\nu C{=}O$, νCOO^-, and νC-N stretching), which suggests the interaction between ARG molecules and the AuNPs. The largest shifts occurred for the bands related to the amino groups, which happens due to changes in the dipole moment of these functional moieties when ARG molecules bind on nanoparticle surface (Aryal et al., 2006). This confirms that NH_2 groups are involved in the AuNPs stabilization, due to the formation of Au-N covalent bonds (Ramezani et al., 2014; Zare et al., 2012) (Fig. S3B).

TEM analysis showed that the nanoparticles were homogeneous in size and mostly spherical in shape, with just a few aggregates (Fig. 1A). The size distribution histogram (Fig. 1B) demonstrated that particles were distributed in the range of 3.0–8.9 nm, with an average particle diameter of 5.5 ± 1.1 nm. Moreover, it was noted that the AuNPs-ARG were close to each other, due to hydrogen bonds between carboxylate and amino groups of ARG in adjacent functionalized nanoparticles (Pu et al., 2013).

DLS showed a unimodal size distribution for AuNPs-ARG, with average hydrodynamic diameters of 12.0 ± 3.2 nm (Fig. S4A). The higher particle diameters observed in this case, when compared to TEM experiments, can be justified considering that DLS measurements give the hydrodynamic diameter as result, whereas TEM provides the effective diameter of the particles in the sample (Lim et al., 2013).

The stability of the AuNPs-ARG suspension was evaluated by performing DLS measurements for one year. The hydrodynamic diameter values did not show any significant variation during this period (Fig. S4B), indicating that nanoparticles were stable. Hence, it is possible to affirm that ARG amino acid is a suitable capping and functionalizing agent.

XRD analysis for AuNPs-ARG (Fig. S5) showed four diffraction peaks at 2θ values of 38.46, 44.70, 65.04, and 78.18 which were assigned to (111), (200), (220) and (311) planes, respectively, of the fcc structure of gold (Li et al., 2012). It can be noted that the diffraction pattern showed some broadening, which is typical for nano-sized crystallites. The calculated lattice constant from (111) diffraction peak was 4.0462 Å, which is in good agreement with the literature (a = 4.0786 Å) (Sen et al., 2013).

3.2. Multivariate optimization of DHEAS immunosensor

To obtain the most suitable conditions to maximize the recognition between IgM and DHEAS antigens on the electrodic surface, three factors – IgM concentration, IgM incubation time and temperature of immunoreaction – were analyzed in the multivariate optimization process. The results obtained in the variable screening, performed by employing a 2^3 full factorial design, are shown in Table S1. The statistical treatment of the experimental data showed that the second order interaction effect between [IgM] and $time_{inc}$, as well as the main effect of immunoreaction temperature, were significant at 95% confidence level (Fig. S6). As the main effect of temperature were positive, it can be said that a higher ΔR_{ct} value is obtained when this variable is adjusted at 37 °C (level +1). This observation is in agreement with several previously reported works, since the interaction between immunoglobulins and antigens is generally favored at this condition (Afkhami et al., 2017; Chen et al., 2016; Li et al., 2018).

The negative second order interaction effect [IgM]*$time_{inc}$ suggests that these variables should be adjusted in opposite levels to obtain a higher response. This behavior can be explained considering that a longer incubation time of the electrodes in IgM solution is necessary for providing a better attachment of the antibody to the *ox*-GCE/AuNPs-ARG. However, a higher [IgM] may not be suitable for the immunosensor construction as it could promote steric hindrance of Fab portions (antigen binding sites) of IgM molecules.

The optimum conditions to the construction of DHEAS immunosensor were obtained by RSM. In this case, [IgM] and incubation time were chosen as variables to perform a 2^2 central composite design (CCD) (central point assayed in triplicate). The levels of such variables were established based on the best conditions observed in the screening step ([IgM] = 1.0 μg dL^{-1} and $time_{inc}$ = 90 min). The immunoreaction temperature was kept at 37 °C, since higher values could result in protein denaturation processes. The experimental matrix is presented in Table S2. The results obtained from CCD were adjusted to a quadratic model, in which the response (ΔR_{ct}) is represented as a function of the

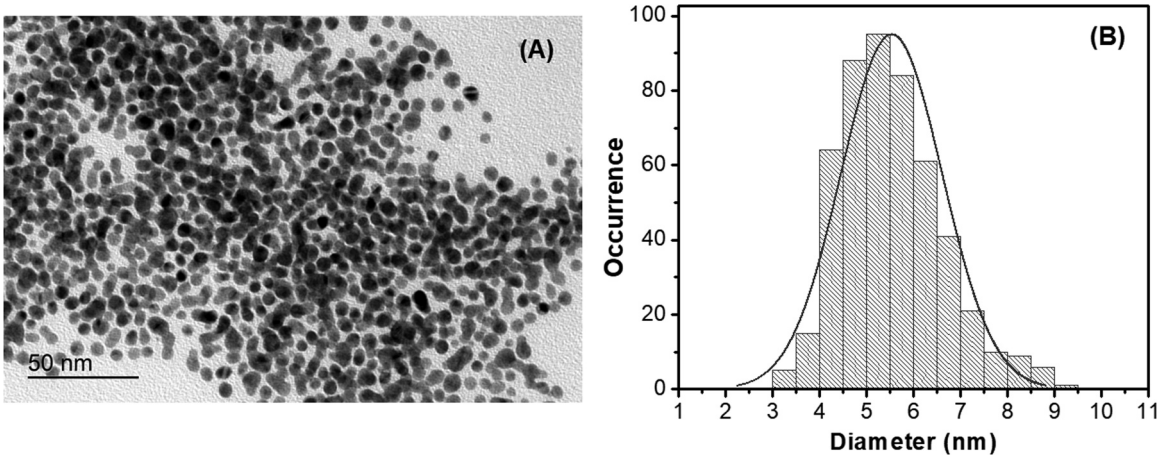

Fig. 1. (A) TEM image of AuNPs-ARG. (B) Particle size distribution histogram.

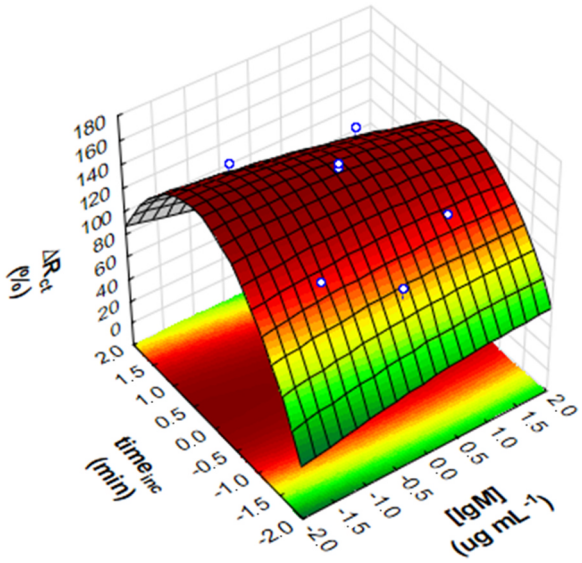

Fig. 2. Response surface plot for ΔR_{ct} as a function of [IgM] and $time_{inc}$.

two studied variables ([IgM] and $time_{inc}$). The resulting equation was:

$$\Delta R_{ct} = 112.45 + 29.09\times[IgM] - 3.89\times([IgM])^2 + 5.63 \times time_{inc} - 0.03\times time_{inc}^2 - 0.32 \times [IgM]\times time_{inc}$$

The statistical significance of the obtained quadratic model was verified by applying analysis of variance (ANOVA) (Table S3). It was found that the regression was statistically significant at 95% confidence level ($F_{Reg} = 19.70 > F_{5,5,95\%} = 5.05$), and that the variability explained by the model was reasonably close to the maximum explainable variation ($R^2 = 0.9164$; Adj-$R^2 = 0.8329$). In addition, no lack of fit (LOF) was observed ($F_{LOF} = 13.98 < F_{3,2,95\%} = 19.16$) and this result was also corroborated by the normality test performed with the residuals ($p > 0.05$). Thus, one can affirm that the proposed quadratic model could explain the experimental data and predict the behavior of the dependent variable (ΔR_{ct}) versus the studied independent variables ([IgM] and $time_{inc}$) with a reliability of 83.3%. The resulting R^2 and Adj-R^2 values are in the acceptable range for data obtained from experiments with biological material (Lundstedt et al., 1998).

The three-dimensional response surface plot related to the quadratic model is shown in Fig. 2. It can be seen that, within the range in which the variables [IgM] and $time_{inc}$ were studied, ΔR_{ct} passes through a maximum region, which corresponds to the optimal experimental zone for the preparation of DHEAS immunosensors. Besides that, it can be observed that the central point of CCD is precisely located in such region; so, these experimental conditions were adopted as the optimal values for immunosensor construction: [IgM] = 1.0 μg mL^{-1} and $time_{inc}$ = 90 min, with immunoassays performed at 37 °C.

3.3. DHEAS immunosensor characterization

Changes in the interfacial properties of the optimized immunosensor resulting from the modification with AuNPs-ARG and biomolecule binding were accompanied by CV and EIS measurements at each step of its construction (Fig. 3).

A *quasi*-reversible voltammetric behavior was exhibited by the electrode at each modification step, which is due to the redox process of $[Fe(CN)_6]^{4-/3-}$. The Nyquist plots presented a semicircle at high frequency region (related to the charge transfer resistance) and the linear region at lower frequencies (attributed to the diffusion-controlled process of the electroactive species in solution) (Bard and Faulkner, 2001).

The *ox*-GCE presented a decrease in the peak currents (I_p) and increases in the peak-to-peak potential separation (ΔE_p) and R_{ct}, compared to the bare GCE. This can be attributed to the formation of oxidized groups on the electrode surface (especially carboxylic groups) (Dekanski et al., 2001; Ghonim et al., 2013; Jarocka et al., 2014), which deprotonate and become negatively charged, hampering the approach of $[Fe(CN)_6]^{3-/4-}$ anions and the electronic transfer process at the electrode/solution interface. This oxidation step was essential to the immunosensor construction, since the generated carboxylic groups could interact effectively with the further immobilized AuNPs-ARG.

The binding of AuNPs-ARG to the *ox*-GCE occurred through the formation of amide bonds between the carboxylate groups of the electrode activated by EDC and NHS and the amine moieties of AuNPs-ARG (Wang et al., 2011). At this step, an increase in I_p values along with decreases in ΔE_p and R_{ct} (Fig. 3) were observed. This behavior is related to the immobilization of AuNPs-ARG, whose high electrical conductivity, high surface area, and electrocatalytic properties could facilitate the charge transfer process on the electrodic surface (Devi et al., 2015; Saha et al., 2012).

For the immobilization of anti-DHEA IgM on *ox*-GCE/AuNPs-ARG, the terminal COO^- groups of Fc fragments of IgM were activated with an EDC/NHS mixture, so that they could bind to the amino groups of the AuNPs-ARG. Oriented IgM anti-DHEA immobilization by Fc portion promotes exposition of Fab domains that are responsible for antigen binding, which enhances the sensitivity and selectivity of the immunosensor (Silva et al., 2013).

After the binding of IgM to the *ox*-GCE/AuNPs-ARG, a decrease in I_p values and increases in ΔE_p and R_{ct} could be noticed (Fig. 3), due to the insulating effect caused by the immobilized immunoglobulins on the electrodic surface. This behavior is an evidence of the suitable binding of such biomolecules to the electrode surface (Karaboğa et al., 2016; Tan et al., 2017; Zhang et al., 2016). After BSA immobilization, an additional decrease in I_p and increments in ΔE_p and R_{ct} were registered, as a consequence of the blocking of immunosensor free sites, thus minimizing nonspecific antigen binding.

3.4. AuNPs-ARG influence

To evaluate the influence of AuNPs-ARG on the immunosensor response, a comparative study was carried out by employing three different configurations: (i) direct immobilization of IgM on the *ox*-GCE (*ox*-GCE/IgM); (ii) binding of IgM to ARG molecules previously immobilized on *ox*-GCE (*ox*-GCE/ARG/IgM); and (iii) immobilization of IgM on AuNPs-ARG (*ox*-GCE/AuNPs-ARG/IgM). In all electrodes, the free sites of the electrode were blocked with BSA. Immunoassays were performed in the presence of 150 μg dL^{-1} DHEAS at 37 °C by using EIS (n = 3), and ΔR_{ct} values obtained after immunoreactions are presented in Fig. S7. It was observed that the ΔR_{ct} values obtained for the *ox*-GCE/IgM and *ox*-GCE/ARG/IgM were substantially lower than those obtained for *ox*-GCE/AuNPs-ARG/IgM. These minor variations may be a consequence of the unsuitable binding of IgM to the electrode, in a way that did not allow the antigen binding sites to remain available for the biomarker recognition. Furthermore, the antibodies might have been bound through weak interactions compared to the covalent bond, favoring their removal during the washing steps or leaching to the electrolyte during the electrochemical measurements. For the AuNPs-ARG based immunosensor, ΔR_{ct} values around 150% were obtained, corroborating that AuNps contributed to an effective immobilization of the antibody molecules, providing a higher number of antigen binding sites for DHEAS detection. This was achieved through the covalent binding of Fc fragment of IgM to AuNPs-ARG, conferring a greater stability and sensitivity to the device.

3.5. Analytical curves

Analytical curves were obtained by EIS under optimized conditions at different concentrations of DHEAS (10.0–110.0 μg dL^{-1}; n = 3). ΔR_{ct} values were linearly dependent on DHEAS concentration according to

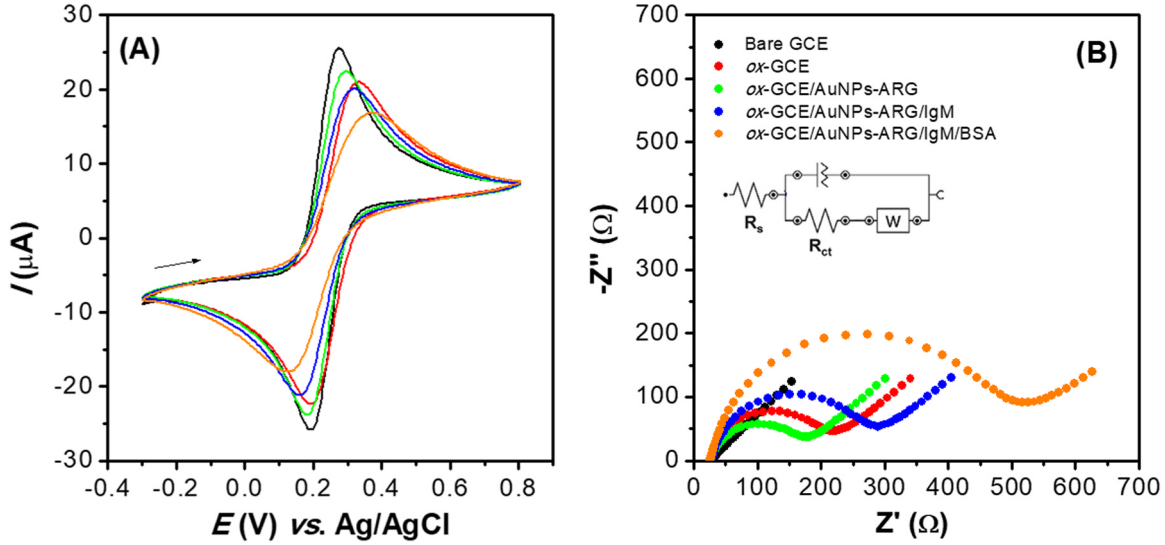

Fig. 3. (A) Cyclic voltammograms and (B) Nyquist diagrams obtained after each step of *ox*-GCE/AuNPs-ARG/IgM construction, in 0.15 mol L^{-1} PBS solution pH 7.4 containing 5.0 mmol L^{-1} $K_4[Fe(CN)_6]/K_3[Fe(CN)_6]$ (same color labels for (A) and (B)).

the following equation: ΔR_{ct} (%) = 30.48 + 0.84 C_{DHEAS} (μg dL^{-1}); R = 0.992; sensitivity = 0.84%Ω/μg dL^{-1}. LOD was found to be equal to 7.4 μg dL^{-1}, which is considered satisfactory for the detection of DHEAS in children aiming the early diagnosis of pACC (normal plasmatic ranges: 2.0–15.0 μg dL^{-1} for 1–5-year-old and 5.0–50.0 μg dL^{-1} for 5–11-year-old subjects) (Mendonça et al., 1995). The *ox*-GCE/AuNPs-ARG/IgM presented an analytical performance similar to some previously reported DHEAS detection methods, such as LC-MS/MS (Chadwick et al., 2005; Sánchez-Guijo et al., 2015; Stener-Victorin et al., 2010), micellar electrokinetic chromatography (Katayama et al., 2003), electrical conductance (Wang et al., 2015), ELISA (Lewis et al., 1996), radioimmunoassay (Lennartsson et al., 2012), and chemiluminescence (Dennedy et al., 2017; Young et al., 1999) (Table S4). Although some DHEAS detection methods present wider linear ranges and lower LOD values compared to the parameters obtained in this work, it is worth mentioning that the *ox*-GCE/AuNPs-ARG/IgM was sensitive enough for monitoring DHEAS aiming the early diagnosis of pACC, considering the typical normal plasmatic ranges. The LOD of 7.4 μg dL^{-1} is comprised within the normal limits, and also the studied linear range covers DHEAS levels that are characteristic for pACC patients. (Fig. 4)

The long-term stability of the developed immunosensor was accessed by measuring EIS responses for 50 μg dL^{-1} DHEAS for one month. Five different immunosensors were equally prepared, and tested in the presence of the biomarker in four different moments: at the day of preparation, and with one, two, three, and four weeks of storage at 4 °C. The initial ΔR_{ct} value (66.7%) did not significantly change up to three weeks of preparation (65.7%, 64.1%, and 67.2% for the first, second and third week of storage, respectively). After this time, the ΔR_{ct} response decreased (48.6%), possibly due to the denaturation of the IgM molecules immobilized on the sensor surface. In spite of that, the reproducible responses observed for the immunosensor in the first three weeks of storage suggests the good stability of the *ox*-GCE/AuNPs-ARG/IgM.

3.6. Interference study

The selectivity of the immunosensor was evaluated by performing EIS measurements before and after immunoassays in the presence of steroid compounds (progesterone, testosterone, and cholesterol), at

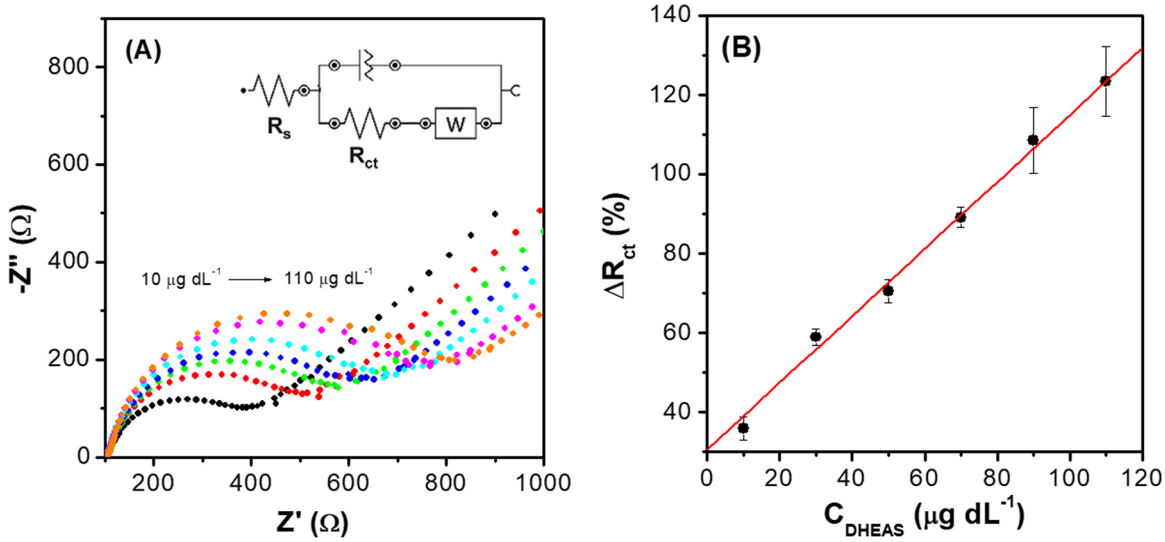

Fig. 4. (A) Nyquist plots obtained with *ox*-GCE/AuNPs-ARG/IgM at different concentrations of DHEAS (0.0, 10.0, 30.0, 50.0, 70.0, 90.0, and 110.0 μg dL^{-1}), in 0.15 mol L^{-1} PBS solution at pH 7.4 containing 5.0 mmol L^{-1} $K_4[Fe(CN)_6]/K_3[Fe(CN)_6]$. (B) Analytical curve obtained for the detection of DHEAS (n = 3).

Table 1
Results for the detection of DHEAS in patient plasma samples by using chemiluminescence and the proposed impedimetric immunosensor (n = 3).

Plasma sample	Chemiluminescence (μg dL^{-1})	EIS[a] (μg dL^{-1})	RSD (%)	Relative error (%)
A	56.0	51.9	3.4	7.3
B	122.0	130.2	4.8	7.7
C	209.0	192.4	3.8	7.9

[a] Average of three determinations.

concentrations corresponding to their normal plasmatic levels in children (American Academy of Pediatrics, 1998; Severson et al., 2017; Sippell et al., 1980). The obtained results (n = 3) were compared to those previously obtained in the presence of 70 μg dL^{-1} DHEAS (Table S5). Low increases in R_{ct} were observed after incubation of the immunosensor in progesterone (6.37%), testosterone (4.10%), and cholesterol (0.84%) solutions, compared to the values obtained in the presence of DHEAS (89.0%), which indicates that the immunosensor is specific for DHEAS. The studied concentrations of the interfering compounds were relatively high for children, and even in this conditions, ΔR_{ct} values were lower than those obtained for DHEAS. These results stated that the immunosensor was satisfactorily specific to detect the studied pACC biomarker.

3.7. Accuracy and reproducibility studies

To evaluate the accuracy and reproducibility of *ox*-GCE/AuNPs-ARG/IgM, samples of fetal bovine serum (FBS) were spiked with different concentrations of the biomarker, followed by immunoassays at 37 °C and EIS measurements (n = 3). The proposed immunosensor presented accuracy and reproducibility for DHEAS detection (Table S6), since acceptable percentage recoveries (94.5–105.3%), %bias (2.43–5.45%), and %RSD (3.99–9.98%) were obtained (Shah et al., 1992, 2000). Moreover, it is important to highlight that the FBS matrix seemed not to influence the analytical performance of the immunosensor.

3.8. Clinical sample analysis

To verify the performance of the *ox*-GCE/AuNPs-ARG/IgM at detecting DHEAS in clinical samples, immunoassays were carried out by EIS in real patient plasma and the resulting levels were compared to the values found with the reference chemiluminescence method (Table 1). The results obtained with the *ox*-GCE/AuNPs-ARG/IgM (n = 3) are in close agreement with those determined by the official methodology. Two-tailed paired *t*-test was applied to these results, and it was demonstrated that there was not statistical difference between the concentrations found with both methods at 95% confidence level (critical *t* value = 4.303; calculated *t* value = −0.582; p (0.619) > 0.050). Hence, the results clearly indicate the promising analytical performance of the developed immunosensor at detecting DHEAS in clinical samples.

4. Conclusions

In this work, a promising and effective label-free impedimetric immunosensor was developed for detection of pACC-related biomarker DHEAS in clinical samples. Arginine-functionalized gold nanoparticles were synthesized by a simple and green route, and used as the chemical modifier of oxidized glassy carbon electrodes. The resultant platform showed to be appropriate for anti-DHEA IgM monoclonal antibodies immobilization. After the multivariate optimization of the electrode construction, the immunosensor could efficiently detect DHEAS by using EIS in the range from 10.0–110.0 μmol L^{-1}, with a LOD of 7.4 μg dL^{-1}. The *ox*-GCE/AuNPs-ARG/IgM showed accuracy, precision and it was specific for the DHEAS determination, enabling the analysis in patient plasma samples. The found results did not show statistical difference when compared to those obtained with the reference chemiluminescence assay. Some important features presented by the proposed device such as label-free approach, simple immunoassay procedure, and possibility of miniaturization can reduce the cost of the immunoassays and enable their future applications to support the early diagnosis of pACC. This sensor construction strategy could also be applied for the modification of disposable screen-printed electrodes for the development of point-of-care systems.

Acknowledgements

This work was financially supported by Coordenação de Aperfeiçoamento de Pessoal de Nível Superior (CAPES, Brazil), Conselho Nacional de Desenvolvimento Científico e Tecnológico (CNPq, Brazil), and Fundação Araucária (Brazil). The authors acknowledge C-LABMU Institutional Laboratory and State University of Ponta Grossa (Ponta Grossa, Paraná, Brazil); Professor Dr. Aldo Zarbin, MSc. João Paulo Vita Damasceno, BSc. Maria Karolina Ramos from Federal University of Paraná (UFPR); Pelé Pequeno Príncipe Research Institute and Pequeno Príncipe Hospital (Curitiba, Paraná, Brasil).

Declaration of interests

None.

Appendix A. Supporting information

Supplementary data associated with this article can be found in the online version at doi:10.1016/j.bios.2019.02.063.

References

Abdel-Khalik, J., Björklund, E., Hansen, M., 2013. J. Chromatogr. B: Anal. Technol. Biomed. Life Sci. 928, 58–77.
Afkhami, A., Hashemi, P., Bagheri, H., Salimian, J., Ahmadi, A., Madrakian, T., 2017. Biosens. Bioelectron. 93, 124–131.
Agência Nacional de Vigilância Sanitária (ANVISA), 2003. Guia para Validação de Métodos Analíticos e Bioanalíticos. Ministério da Saúde, Brasil (Resolução (RE) nº 889, de 29/05/2003).
American Academy of Pediatrics, 1998. Pediatrics 101, 141–147.
Arakawa, H., Maeda, M., Tsuji, A., Kambegawa, A., 1981. Steroids 38, 453–464.
Aryal, S., Remant, B.K.C., Dharmaraj, N., Bhattarai, N., Kim, C.H., Kim, H.Y., 2006. Spectrochim. Acta Part A 63, 160–163.
Austin, L.A., Mackey, M.A., Dreaden, E.C., El-Sayed, M.A., 2014. Arch. Toxicol. 88, 1391–1417.
Ayala-Ramirez, M., Jasim, S., Feng, L., Ejaz, S., Deniz, F., Busaidy, N., Waguespack, S.G., Naing, A., Sircar, K., Wood, C.G., Pagliaro, L., Jimenez, C., Vassilopoulou-Sellin, R., Habra, M.A., 2013. Eur. J. Endocrinol. 169, 891–899.
Bard, A.J., Faulkner, L.R., 2001. Electrochemical Methods: Fundamentals and Applications, Second ed. John Wiley & Sons, New York.
Büttler, R.M., Martens, F., Kushnir, M.M., Ackermans, M.T., Blankenstein, M.A., Heijboer, A.C., 2015. Clin. Chim. Acta 438, 157–159.
Carneiro, P., Loureiro, J., Delerue-Matos, C., Morais, S., Pereira, M.C., 2017. Sens. Actuators B 239, 157–165.
Cavagnini, F., Giraldi, F.P., 2016. Adrenal causes of Cushing's syndrome. In: Jameson, J.L., Groot, L.J., Giudice, L.C., Grossman, A.B., Kretser, D., Melmed, S., Potts JrJ.T., Weir, G.C. (Eds.), Seventh ed. Endocrinology: Adult and Pediatric Volume II. Saunders/Elsevier Inc., Philadelphia, pp. 1775–1809.
Chadwick, C.A., Owen, L.J., Keevil, B.G., 2005. Ann. Clin. Biochem. 42, 468–474.
Chen, Y., Li, Y., Deng, D., He, H., Yan, X., Wang, Z., Fan, C., Luo, L., 2018. Biosens. Bioelectron. 15, 301–306.
Chen, Q., Yu, C., Gao, R., Gao, L., Li, Q., Yuan, G., He, J., 2016. Biosens. Bioelectron. 79, 364–370.
Custódio, G., Parise, G.A., Kiesel Filho, N., Komechen, H., Sabbaga, C.C., Rosati, R., Grisa, L., Parise, I.Z.S., Pianovski, M.A.D., Fiori, C.M.C.M., Ledesma, J.A., Barbosa, J.R.S., Figueiredo, F.R.O., Sade, E.R., Ibañez, H., Arram, S.B.I., Stinghen, S.T., Mengarelli, L.R., Figueiredo, M.M.O., Carvalho, D.C., Avilla, S.G.A., Woiski, T.D., Poncio, L.C., Lima, G.F.R., Pontarolo, R., Lalli, E., Zhou, Y., Zambetti, G.P., Ribeiro, R.C., Figueiredo, B.C., 2013. J. Clin. Oncol. 31, 2619–2626.
Damgaard-Olesen, A., Johannsen, T.H., Holmboe, S.A., Søeborg, T., Petersen, J.H., Andersson, A.M., Aadahl, M., Linneberg, A., Juul, A., 2016. Clin. Chim. Acta 454, 82–88.
Dekanski, A., Stevanović, J., Stevanović, R., Nikolić, B.Ž., Jovanović, V.M., 2001. Carbon 39, 1195–1205.

Dennedy, M.C., Annamalai, A.K., Prankerd-Smith, O., Freeman, N., Vengopal, K., Graggaber, J., Koulouri, O., Powlson, A.S., Shaw, A., Halsall, D.J., Gurnell, M., 2017. J. Clin. Endocrinol. Metab. 102, 786–792.
Devi, R.V., Doble, M., Verma, R.S., 2015. Biosens. Bioelectron. 68, 688–698.
DiGiammarino, E.L., Lee, A.S., Cadwell, C., Zhang, W., Bothner, B., Ribeiro, R.C., Zambetti, G., Kriwacki, R., 2002. Nat. Struct. Biol. 9, 12–16.
Doghman, M., Wakil, A.E., Cardinaud, B., Thomas, E., Wang, J., Zhao, W., Peralta-Del Valle, M.H., Figueiredo, B.C., Zambetti, G.P., Lalli, E., 2010. Tumor Stem Cell Biol. 70, 4666–4675.
Else, T., Kim, A.C., Sabolch, A., Raymond, V.M., Kandathil, A., Caoili, E.M., Jolly, S., Miller, B.S., Giordano, T.J., Hammer, G.D., 2014. Endocr. Rev. 35, 282–326.
Engelbrekt, C., Sørensen, K.H., Zhang, J., Welinder, A.C., Jensen, P.S., Ulstrup, J., 2009. J. Mater. Chem. 19, 7839–7847.
Fassnacht, M., Libé, R., Kroiss, M., Allolio, B., 2011. Nat. Rev. Endocrinol. 7, 323–335.
Fay, A.P., Elfiky, A., Teló, G.H., McKay, R.R., Kaymakcalan, M., Nguyen, P.L., Vaidya, A., Ruan, D.T., Bellmunt, J., Choueiri, T.K., 2014. Crit. Rev. Oncol./Hematol. 92, 123–132.
Fett-Conte, A.C., Salles, A.B.C.F., 2002. Rev. Bras. De. Hematol. e Hemoter. 24, 85–89.
Fogaça, R.L., Alvarenga, L.M., Woiski, T.D., Becker-Finco, A., Teixeira, K.N., Silva, S.K., Moraes, R.N., Noronha, L., Noiray, M., Figueiredo, B.C., Billiald, P., Moura, J., 2019. Nanomedicine. https://doi.org/10.2217/nnm-2018-0230.
Ghonim, A.M., El-Anadouli, B.E., Saleh, M.M., 2013. Electrochim. Acta 114, 713–719.
Guan, J., Wang, Y., Gunasekaran, S., 2015. J. Food Sci. 80, N828–N833.
Guran, T., Firat, I., Yildiz, F., Bulut, I.K., Dogru, M., Berekett, A., 2015. Clin. Endocrinol. 82, 712–718.
International Conference on Harmonisation (ICH), 2005. Harmonised Tripartite Guideline. Validation of Analytical Procedures: Text and Methodology Q2 (R1).
Jarocka, U., Sawicka, R., Góra-Sochacka, A., Sirko, A., Zagórski-Ostoja, W., Radecki, J., Radecka, H., 2014. Biosens. Bioelectron. 55, 301–306.
Karaboğa, M.N.S., Şimşek, Ç.S., Sezgintürk, M.K., 2016. Biosens. Bioelectron. 84, 22–29.
Katayama, M., Matsuda, Y., Shimokawa, K., Kaneko, S., 2003. Biomed. Chromatogr. 17, 263–267.
Kumar, B., Bhalla, V., Bhadoriya, R.P.S., Suri, C.R., Varshney, G.C., 2016. RSC Adv. 6, 75862–75869.
Kumar, N., Upadhyay, L., 2016. Appl. Surf. Sci. 385, 225–233.
Lalli, E., Figueiredo, B.C., 2015. Front. Endocrinol. 06 (article 23).
Lennartsson, A., Kushnir, M.M., Bergquist, J., Jonsdottir, I.H., 2012. Biol. Psychol. 90, 143–149.
Lewis, J.G., Bason, L.M., Elder, P.A., 1996. Steroids 61, 682–687.
Li, C.C., Chen, L.B., Li, Q.H., Wang, T.H., 2012. CrystEngComm 14, 7549–7551.
Li, Y., He, J., Chen, J., Niu, Y., Zhao, Y., Zhang, Y., Yu, C., 2018. Biosens. Bioelectron. 101, 7–13.
Liang, X., Wang, Z., Liu, C., 2010. Nanoscale Res. Lett. 5, 124–129.
Lim, J., Yeap, S.P., Che, H.X., Low, S.C., 2013. Nanoscale Res. Lett. 8, 1–14 (article 381).
Luna, D.M.N., Avelino, K.Y.P.S., Cordeiro, M.T., Andrade, C.A.S., Oliveira, M.D.L., 2015. Sens. Actuators, B 220, 565–572.
Lundstedt, T., Seifert, E., Abramo, L., Thelin, B., Nyström, Å., Pettersen, J., Bergman, R., 1998. Chemom. Intell. Lab. Syst. 42, 3–40.
Mayya, K.M., Jain, N., Gole, A., Langevin, D., Sastry, M., 2004. J. Colloid Interface Sci. 270, 133–139.
Mendonça, B.B., Lucon, A.M., Menezes, C.A.V., Saldanha, L.B., Latronico, A.C., Zerbini, C., Madureira, G., Domenice, S., Albergaria, M.A.P., Camargo, M.H.A., Halpern, A., Liberman, B., Arnhold, I.J.P., Bloise, W., Andriolo, A., Nicolau, W., Silva, F.A.Q., Wroclaski, E., Arap, S., Wajchenberg, B.L., 1995. J. Urol. 154, 2004–2009.
Monerris, M.J., D'Eramo, F., Arévalo, F.J., Fernández, H., Zon, M.A., Molina, P.G., 2016. Microchem. J. 129, 71–77.
Nelson, D.J., Cox, M., 2005. Lehninger Principles of Biochemistry, fourth ed. W.H. Freeman and Company, New York.
Pacławski, K., Streszewski, B., Jaworski, W., Luty-Błocho, M., Fitzner, K., 2012. Colloids Surf. A 413, 208–215.
Pires, N.M.M., Dong, T., Hanke, U., Hoivik, N., 2014. Sensors 14, 15458–15479.
Pretsch, E., Bühlmann, P., Badertscher, M., 2009. Structure Determination of Organic Compounds: Tables of Spectral Data, fourth ed. Springer, Berlin.
Przytulska, J., Rogala, N., Bednarek-Tupikowska, G., 2015. Adv. Clin. Exp. Med. 24, 185–193.
Pu, W., Zhao, H., Huang, C., Wu, L., Xu, D., 2013. Anal. Chim. Acta 764, 78–83.
Rama, E.C., Costa-García, A., 2016. Electroanalysis 28, 1700–1715.
Ramezani, F., Amanlou, M., Rafii-Tabar, H., 2014. Amino Acids 46, 911–920.
Ribeiro, R.C., Sandrini, F., Figueiredo, B., Zambetti, G.P., Michalkiewicz, E., Lafferty, A.R., DeLacerda, L., Rabin, M., Cadwell, C., Sampaio, G., Cat, I., Stratakis, C.A., Sandrini, R., 2001. Proc. Natl. Acad. Sci. USA 98, 930–9335.
Ronchi, C.L., Kroiss, M., Sbiera, S., Deutschbein, T., Fassnacht, M., 2014. Eur. J. Endocrinol. 171, R1–R11.
Saha, K., Agasti, S.S., Kim, C., Li, X., Rotello, V.M., 2012. Chem. Rev. 112, 2739–2779.
Sánchez-Guijo, A., Oji, V., Hartmann, M.F., Traupe, H., Wudy, S.A., 2015. J. Lipid Res. 56, 1843–1851.
Sen, I.K., Maity, K., Islam, S.S., 2013. Carbohydr. Polym. 91, 518–528.
Severson, A., Barclay, S., Kim, S., 2017. Testosterone levels by age. Extracted from: 〈http://www.healthline.com/health/low-testosterone/testosterone-levels-by-age#Overview1〉, in 06/22/2018.
Shah, V.P., Midha, K.K., Dighe, S., McGilveray, I.J., Skelly, J.P., Yacobi, A., Layloff, T., Viswanathan, C.T., Cook, C.E., McDowall, R.D., Pittman, K.A., Spector, S., 1992. Int. J. Pharm. 82, 1–7.
Shah, V.P., Midha, K.K., Findlay, J.W.A., Hill, H.M., Hulse, J.D., McGilveray, I.J., McKay, G., Miller, K.J., Patnaik, R.N., Powell, M.L., Tonelli, A., Viswanathan, C.T., Yacobi, A., 2000. Pharm. Res. 17, 1551–1557.
Shibata, Y., Arai, S., Honma, S., 2015. J. Steroid Biochem. Mol. Biol. 145, 193–199.
Shrivastav, T.G., Chaube, S.K., Kariya, K.P., Kumar, D., Singh, R., 2011a. J. Immunoass. Immunochem. 32, 326–341.
Shrivastav, T.G., Chaube, S.K., Kariya, K.P., Kumar, D., Singh, R., 2011b. J. Immunoass. Immunochem. 32, 114–127.
Silva, B.V.M., Cavalcanti, I.T., Silva, M.M.S., Dutra, R.F., 2013. Talanta 117, 431–437.
Sippell, W.G., Döhr, H.G., Bidlingmaier, F., Knorr, D., 1980. Pediatr. Res. 14, 39–46.
Stener-Victorin, E., Holm, G., Labrie, F., Nilsson, L., Janson, P.O., Ohlsson, C., 2010. J. Clin. Endocrinol. Metab. 95, 810–819.
Sun, B., Gou, Y., Ma, Y., Zheng, X., Bai, R., Abdelmoaty, A.A.A., Hu, F., 2017. Biosens. Bioelectron. 88, 55–62.
Suvarna, S., Das, U., Sunil, K.C., Mishra, S., Sudarshan, M., Saha, K.D., Dey, S., Chakraborty, A., Narayana, Y., 2017. PLoS One 12, 1–15.
Tan, Y., Wang, Y., Li, M., Ye, X., Wu, T., Li, C., 2017. Biosens. Bioelectron. 91, 741–746.
Wan, Y., Su, Y., Zhu, X., Liu, G., Fan, C., 2013. Biosens. Bioelectron. 47, 1–11.
Wang, C., Yan, Q., Liu, H., Zhou, X., Xiao, S., 2011. Langmuir 27, 12058–12068.
Wang, C., Kim, J., Zhu, Y., Yang, J., Lee, G., Lee, S., Yu, J., Pei, R., Liu, G., Nuckolls, C., Hone, J., Lin, Q., 2015. Biosens. Bioelectron. 71, 222–229.
Yang, X., Samanta, B., Agasti, S.S., Jeong, Y., Zhu, Z., Rana, S., Miranda, O.R., Rotello, V.M., 2011. Angew. Chem. Int. Ed. 50, 477–481.
Young, D.G., Skibinski, G., Mason, J.I., James, K., 1999. Clin. Exp. Immunol. 117, 476–481.
Zare, D., Akbarzadeh, A., Barkhi, M., Khoshnevisan, K., Bararpour, N., Noruzi, M., Tabatabaei, M., 2012. Synth. React. Inorg. Met. -Org. Nano-Met. Chem. 42, 266–272.
Zhang, X., Zhou, D., Sheng, S., Yang, J., Chen, X., Xie, G., Xiang, H., 2016. Microchim. Acta 183, 2055–2062.
Zhang, X., Wang, H., Coulter, J.A., Yang, R., 2018. Int. J. Nanomed. 13, 3541–3552.